Optimal Transport and *h*-adaptive based mesh generation for the Poisson equation in non-convex domains

Simone Appella, Chris Budd and Tristan Pryer

September 10, 2021

Abstract

In this paper, we solve the Poisson equation using the discontinuous Galerkin method on two non-convex domains discretised with an *h-adaptive* and *Optimal Transport* based mesh strategy. The *h*-refinement strategy will be guided by an L^2 and L^∞ *a-posteriori* estimates and will display numerically optimal convergence rate. We devise the Optimal Transport mesh by considering the local behaviour of the solution near the re-entrant corner. This procedure results in the solution of a one-dimensional algebraic equation, computationally less expensive than the standard approach of solving the fully Monge-Ampère equation. Our proposed method requires the specification of a hyper-parameter, which affects the accuracy of the Galerkin method and the mesh quality. Its critical values yield optimal convergence rate in L^2 and L^∞ and are supported by theoretical proof. Moreover, the resulting mesh is able to equidistribute the a-posteriori estimates. This hints at the close relationship between Optimal Transport and *h*-adaptation for the common goal of equidistributing the local truncation error, which is worth of further theoretical investigation. We conlude by analysing the *skewness* quality measure for the Optimal Transport mesh and show that this metric does locally depend only on the angle of the re-entrant corner.

1 Introduction

Solutions of elliptic boundary value problems defined on non-convex domains display singular behaviour near re-entrant corners. This occurs even when data of the underlying problem are very smooth. Such singular behaviour affects the accuracy of Finite Element Methods (FEMs) throughout the whole domain. Hence, the solutions of the corresponding problems lie typically in Sobolev spaces H^k for small $k > 1$ [BG88; BG89]. The theoretical framework of weighted Sobolev spaces, which were originally studied in [BR72; BKP79] for elasticity and potential problems, can deal with this constraint and will be used for discretising the Poisson equation.

We treat the equation defined on a general non-convex domain with prescribed Dirichlet boundary conditions. The numerical solution of this equation has been already addressed in [ZSG02; SH16; ZS02]. The discretisation is performed with the Symmetric Interior Pentalty discontinuous Galerkin (SIP-dG) method, formulated in [Arn82; Arn+00; Arn+02]. The popularity of the dG method resides in its flexibility with respect to adapted elements of various types and shapes. Though, in all the previous works, error estimates of *h*- or *p*-type under strong regularity assumptions are given. In order to account for the singularities, appropriate adaptive mesh strategies must be carefully selected to obtain optimal convergence rate.

The first contribution of this paper consists in the derivation of an *a-posteriori* estimate in the L^2 norm. The proof relies on the dual weak formulation of the Poisson problem and on the properties of the weighted Sobolev spaces [Wih03; Sch98]. An L^∞ a-posteriori bound will be also used for the subsequent numerical experiments [DG12].

The adapted SIP-dG method will be tested numerically for the two adaptive strategies on the L-shaped and crack domain. The rate of convergence in the L^2 and L^∞ norm for *h*-refinement will be computed using the corresponding a-posteriori bounds. The Optimal Transport (OT) strategy involves the derivation of a local map from a computational to a physical domain in the vicinity of the

re-entrant corner, where the solution of the Poisson equation strongly depends on the radial variable but not on the angular one. This allows us to compute the OT mesh via a one-dimensional non-algebraic equation, less computationally expensive than the fully two-dimensional Monge-Ampère equation. It is though crucial to choose an appropriate value for an hyper-parameter, which controls the level of node clustering near the the re-entrant corner, ultimaltely affecting the accuracy, converge rate of the SIP-dG method and the quality of the mesh. The optimal values in terms of accuracy and convergence rate are obtained by equidistributing a one-dimensional monitor function. We will also evidence the close relationship between the OT strategy and h-refinement, as both aim at equidistributing the a-posteriori monitor functions and for this reason are guided toward the minimisation of the overall truncation error.

The quality of the OT mesh will be assessed with the *skewness* metric. It will be proved theoretically and by numerical tests that it does only depend on the angle of the re-entrant corner and not on the dimension of the FE space.

The remainder of the paper is structured as follows. In §2 we introduce the notation of the weighted Sobolev spaces for the SIP-dG discretisation of the Poisson equation. In §3 we derive the a-posteriori error estimator in the L^2 norm from the dual formulation of the original problem. In §4 we will conduct numerical tests on the L-shaped and crack domain. Initially, we will assess the accuracy of the SIP-dG method genereated on the h-adaptive meshes using the a-posteriori estimates. Then, we will describe the derivation of the Optimal Transport based mesh and evaluate the best hyper-parameter in terms of accuracy and ability to equidistribute the a-posteriori estimates. The last part of this section will investigate the quality of the OT mesh in terms of the skewness metric.

Finally, we will draw our conclusions and propose ideas to further expand our work in §6.

2 Problem setup and discretisation

Let $\Omega \subset \mathbb{R}^2$ be a bounded, polygonal domain with outward unit normal $\vec{n}_\Omega$. Suppose that the boundary $\Gamma = \partial\Omega$ is composed by a Dirichlet part Γ_D with $|\Gamma_D| > 0$ and a Neumann part Γ_N such that:

$$\overline{\Gamma} = \overline{\Gamma}_D \cup \overline{\Gamma}_N. \tag{1}$$

All the vertices are included in the closure. The corner vertices and the points of changing boundary conditions are *singular points* and collected in the set

$$SP(\Omega, \Gamma_D, \Gamma_N) = \{A_i : i = 1, \dots, M\}. \tag{2}$$

The interior opening angle of the domain at A_i is measured anti-clockwise and denoted by $\omega \in (0, 2\pi]$. The case $\omega = \pi$ allows boundary conditions to switch from Neumann to Dirichlet or vice versa.

To account for the regularity of the elliptic problem, suitable Sobolev spaces will be introduced. A weight $\beta_i \in (0, 1]$ is associated with each singular point $A_i \in SP(\Omega, \Gamma_D, \Gamma_N)$ and stored in the vector $\vec{\beta} = (\beta_1, \cdots, \beta_M)$. For any number $k \in \mathbb{R}$, we let

$$\vec{\beta} + k = (\beta_1 + k, \dots, \beta_M + k).$$

We then introduce the weight function on Ω:

$$\Phi_{\vec{\beta}}(\vec{x}) = \prod_{i=1}^{M} r_i(\vec{x})^{\beta_i}, \quad r_i(\vec{x}) = |\vec{x} - A_i|.$$

Then, for any integers $m \geq l \geq 0$, the weighted Sobolev spaces $\mathrm{H}^{m,l}_{\vec{\beta}}(\Omega)$ are defined as completion of the space $C^\infty(\overline{\Omega})$ with respect to the weighted Sobolev norms

$$\|u\|^2_{\mathrm{H}^{m,l}_{\vec{\beta}}(\Omega)} = \|u\|^2_{\mathrm{H}^{l-1}(\Omega)} + |u|^2_{\mathrm{H}^{m,l}_{\vec{\beta}}(\Omega)}, \quad l \geq 1$$
$$\|u\|^2_{\mathrm{H}^{m}_{\vec{\beta}}(\Omega)} = \sum_{\substack{|\alpha|=k \\ k=0}}^{m} \left\| |D^\alpha u| \Phi_{\vec{\beta}+k} \right\|^2_{\mathrm{L}^2(\Omega)}, \quad l = 0, \tag{3}$$

where

$$|u|^2_{\mathrm{H}^{m,l}_{\vec{\beta}}(\Omega)} = \sum_{\substack{|\alpha|=k \\ k=l}}^{m} \left\| |D^\alpha u| \Phi_{\vec{\beta}+k-l} \right\|^2_{\mathrm{L}^2(\Omega)}$$

and

$$D^\alpha u = \frac{\partial^{|\alpha|} u}{\partial x_1^{\alpha_1} \partial x_2^{\alpha_2}},$$

with $\alpha = (\alpha_1, \alpha_2) \in \mathbb{N}^2$ and $|\alpha| = \alpha_1 + \alpha_2$.

Fractional Sobolev spaces for $m \in \mathbb{R}$ appear naturally as the correct range of the continuous trace map

$$\tau : \mathrm{H}^m(\Omega) \to \mathrm{H}^{m-1/2}(\Gamma), \quad m > 1/2,$$

and will be used to define properly the boundary conditions for the Poisson problem.

We mention the following remark proved in [Wih03]:

Remark 1 (Properties of the weighted Sobolev spaces [Wih03, Remark 1.2.2]) *The following properties hold:*

1. *If $u \in \mathrm{H}^{m,m}_{\vec{\beta}}(\Omega)$, $m \geq 0$, then $u \in \mathrm{H}^m(\Omega_0)$ for all domains $\Omega_0 \subset \Omega$ with*
$$P \notin \overline{\Omega_0} \qquad \forall\, P \in SP(\Omega, \Gamma_D, \Gamma_N).$$
2. *Although $\mathrm{H}^{2,2}_{\vec{\beta}}(\Omega) \not\subset \mathrm{H}^2(\Omega)$, it was proven in [BKP79] that $\mathrm{H}^{2,2}_{\vec{\beta}}(\Omega) \subset \mathscr{C}^0(\overline{\Omega})$.*
3. *For $u \in \mathrm{H}^{2,2}_{\vec{\beta}}(\Omega)$, there holds $\nabla u \in \mathrm{H}^{1,1}_{\vec{\beta}}(\Omega)^2$.*

2.1 Poisson equation in 2D

Let $\Omega \subset \mathbb{R}^2$ be a bounded, polygonal domain. Consider the following *Poisson problem*

$$\begin{aligned} -\Delta u &= f \text{ in } \Omega \\ u &= u_D \text{ on } \Gamma_D \\ \nabla u \cdot \vec{n}_\Omega &= g \text{ on } \Gamma_N. \end{aligned} \tag{4}$$

Here, f is a given datum lying on the dual space of $\mathrm{H}^1_0(\Omega)$ and denoted by $\mathrm{H}^{-1}(\Omega)$, $u_D \in \mathrm{H}^{1/2}(\Gamma_D)$ and $g \in \mathrm{H}^{-1/2}(\Gamma_N)$ are prescribed Dirichlet and Neumann boundary conditions, respectively. In the framework of weighted Sobolev spaces, the existence and uniqueness of problem (4) is stated in the following Theorem:

Theorem 2 (Regularity of the Poisson equation [BG88, Theorem 3.1]) *Let Ω be a polygon in $\mathbb{R}^2$ and $m \geq 0$ a given integer. Then, there exists a weight vector $\vec{\beta}_{min}$ with $0 \leq \vec{\beta}_{min} < 1$ depending on the opening angles at the vertices $A_i \in SP(\Omega, \Gamma_D, \Gamma_N)$, such that for weight vectors $\vec{\beta}$ with $\vec{\beta}_{min} \leq \vec{\beta} < 1$ and for*

$$f \in \mathrm{H}^{m,0}_{\vec{\beta}}(\Omega),\ u_D \in \mathrm{H}^{m+3/2,3/2}_{\vec{\beta}}(\Gamma_D),\ g \in \mathrm{H}^{m+1/2,1/2}_{\vec{\beta}}(\Gamma_N),$$

the problem (4) has a unique solution $u \in \mathrm{H}^{m+2,2}_{\vec{\beta}}(\Omega)$.

Remark 3 ([BG88, Theorem 2.1 - Remark 3]) *In the case of the Poisson equation the value of* $\vec{\beta}_{min}$ *is well-known at each corner* A_i *and given by*

$$\beta_{min,i} = \begin{cases} 1 - \frac{\pi}{\omega} & \text{if } \overline{A_i A_{i+1}} \in \Gamma_D \text{ or } \Gamma_N, \\ 1 - \frac{\pi}{2\omega} & \text{otherwise.} \end{cases} \tag{5}$$

2.2 Finite element spaces

Let $\mathscr{T}$ be a conforming mesh of Ω into simplicial open elements K:

$$\mathscr{T} = \{K_i\}_i, \quad \bigcup_{K \in \mathscr{T}} \overline{K} = \overline{\Omega}.$$

We consider $\mathscr{T}$ is a finite family of sets such that:

1. $K \in \mathscr{T}$ implies K is an open triangle or quadrilateral,
2. for any $K, J \in \mathscr{T}$ we have that $\overline{K} \cap \overline{J}$ is either empty or a complete $(2-r)$-dimensional simplex/box (i.e., it is either a vertex for $r = 2$, or an edge for $r = 1$, or the whole of $\overline{K}$ and $\overline{J}$) of both $\overline{K}$ and $\overline{J}$,
3. $\bigcup_{K \in \mathscr{T}} \overline{K} = \overline{\Omega}$.

Additionally, for each $K \in \mathscr{T}$ we introduce

$$h_K = diam(K) := sup_{x,y \in K} |x - y|$$

and

$$\rho_K = sup\{diam(B) : B \text{ is an open ball contained in } K\}.$$

Finally, the maximum and minimum *mesh width* of $\mathscr{T}$ is given by

$$\overline{h} = \max_{K \in \mathscr{T}} h_K, \quad \underline{h} = \min_{K \in \mathscr{T}} h_K.$$

We will also assume that all the meshes generated by the h-,r- refinement are *shape regular*. Let $\mathscr{G} = \{\mathscr{T}_i\}_{i \in \mathbb{N}}$ be a family of meshes, then $\mathscr{G}$ is characterised by the shape regularity $\mu(\mathscr{T})$ if

$$\mu(\mathscr{T}) = \min_{K \in \mathscr{T}_i} \frac{h_K}{\rho_K} > 0. \tag{6}$$

The set of all edges of $\mathscr{T}$ is denoted by $\mathscr{E}$, which we partition into subsets $\mathscr{E}_D, \mathscr{E}_N, \mathscr{E}_I$, consisting of edges lying on the Dirichlet boundary Γ_D, the Neumann boundary Γ_N, and the interior edges, respectively. The corresponding quantities for each individual element K are denoted by $\mathscr{E}(K)$, $\mathscr{E}_D(K)$, $\mathscr{E}_N(K)$, $\mathscr{E}_I(K)$, respectively.

We split the index set $\{1, \dots, M\}$ of boundary edges e_i into $\mathscr{D}$ and $\mathscr{N}$, on which Dirichlet and Neumann boundary conditions are applied, respectively. This leads to $\overline{\Gamma}_D = \bigcup_{i \in \mathscr{D}} \overline{e}_i$ and $\overline{\Gamma}_N = \bigcup_{i \in \mathscr{N}} \overline{e}_i$.

We define the *finite element space*

$$\mathbb{V} := \{v \in \mathrm{L}^2(\Omega) : v|_K \in \mathbb{P}^p(K) \qquad \forall\, K \in \mathscr{T}\}, \tag{7}$$

where $\mathbb{P}^p(K)$ is the space of polynomials of total degree p.

We remark that the space $\mathbb{V}$ does not carry any inter-element continuity and does not encode any boundary condition. These will be enforced weakly in the variational scheme. Given an edge γ of $\mathscr{T}$, we define the *jump* and *average* operator of $v \in \mathbb{V}$ on the edges $\mathscr{E}$ at $\vec{x} \in \gamma$ by

$$[\![v]\!] := \begin{cases} v|_K \vec{n}_K + v|_{K'} \vec{n}_{K'} \\ v|_K \vec{n}_\Omega \end{cases} \qquad [\![\vec{v}]\!] := \begin{cases} \vec{v}|_K \cdot \vec{n}_K + \vec{v}|_{K'} \cdot \vec{n}_{K'} & \text{on } \gamma = \partial K \cap \partial K' \\ \vec{v}|_K \cdot \vec{n}_\Omega & \text{on } \gamma = \partial K \cap \Gamma_D \end{cases} \tag{8}$$

$$\{\!\{ v \}\!\} := \begin{cases} \frac{1}{2}(v|_K + v|_{K'}) \\ v|_K \end{cases} \qquad \{\!\{ \vec{v} \}\!\} := \begin{cases} \frac{1}{2}(\vec{v}|_K + \vec{v}|_{K'}) & \text{on } \gamma = \partial K \cap \partial K' \\ \vec{v}|_K & \text{on } \gamma = \partial K \cap \Gamma_D \end{cases} \tag{9}$$

Here $v|_K$ denotes the trace of v onto the edge $\gamma \in \mathscr{E}(K) \cap \mathscr{E}(K')$ and $\vec{n}_K$ is the outward unit vector relative to K on γ. For $\gamma \subset \Gamma$, we define $\{\!\{ v \}\!\} := v$, $\{\!\{ \vec{v} \}\!\} := \vec{v}$, $[\![v]\!] := v\vec{n}_\Omega$, and $[\![\vec{v}]\!] := \vec{v} \cdot \vec{n}_\Omega$.

Using the jump and average operator we introuce the mesh condition $q(\mathscr{T})$ as an alternative quality measure. Under the condition

$$q := \| [\![h]\!] / \{\!\{ h \}\!\} \|_{\mathrm{L}^\infty(\mathscr{E}_I)} \leq \alpha, \quad 0 \leq \alpha < 1 \text{ small enough}, \tag{10}$$

it has been shown that the inf-sup stability of the bilinear form given by the weak formulation of the Poisson equation holds [GMP17].

To account for the singular behaviour of solutions near singular points of the polygon Ω, we define the set

$$\mathscr{K}_0 = \{K \in \mathscr{T} : P \in \overline{K} \text{ for some } P \in SP(\Omega, \Gamma_D, \Gamma_N)\}. \tag{11}$$

Let $K \in \mathscr{K}_0$. We will assume the mesh is graded enough such that exactly one singular point belongs to $\overline{K}$. The corresponding vertex is denoted by A_K and the corresponding weight β_K. Moreover, the spaces $\mathrm{H}^{m,l}_{\beta_k}(K)$ are equipped with the weight function $\Phi_{\beta_K}(\vec{x}) = r_K^{\beta_K}$, where $r_K = |\vec{x} - A_K|$.
We conclude the section by stating the following lemmas [Wih03]:

Lemma 4 (Trace inequalities [Wih03, Lemma A.2.4]) *Let $\gamma \in \mathscr{E}(K)$. Then, there holds*

1. *if $u \in \mathrm{H}^2(K)$ and $u = 0$ at the vertices of K, then the trace $u|_\gamma \in \mathrm{H}^1(\gamma)$ and*

$$\begin{aligned} \|u\|^2_{\mathrm{H}^1(\gamma)} &\leq C h_K \, |u|^2_{\mathrm{H}^2(K)} \\ \|u\|^2_{\mathrm{L}^2(\gamma)} &\leq C h_K^3 \, |u|^2_{\mathrm{H}^2(K)} . \end{aligned} \tag{12}$$

2. *if $u \in \mathrm{H}^{2,2}_{\vec{\beta}}(\Omega)$, $0 < \beta < 1$, and $u = 0$ at the vertices of K, then*

$$\begin{aligned} \|u\|^2_{\mathrm{H}^1(\gamma)} &\leq C h_K^{1-2\beta} |u|^2_{\mathrm{H}^{2,2}_\beta(K)} \\ \|u\|^2_{\mathrm{L}^2(\gamma)} &\leq C h_K^{3-2\beta} \, |u|^2_{\mathrm{H}^{2,2}_\beta(K)}, \end{aligned} \tag{13}$$

   if γ does not contain any vertex A_i, $i = 1, \ldots, M$.

Lemma 5 (Continuity at the interior edges [Wih03, Lemma 1.3.4]) *Let $u \in \mathrm{H}^{1,1}_{\vec{\beta}}(\Omega)$ for $0 \leq \vec{\beta} \leq 1$. Then, for an interior edge $\gamma \in \mathscr{E}_I$ there holds $[\![u]\!] = 0$ a.e. on γ.*

2.3 Variational formulation of the Poisson equation

Here, we define the SIP-dG variational formulation of problem (4) and state its consistency.

Definition 2.1 (SIP-dG of the Poisson equation) *Define the bilinear form $\mathscr{A}_h$ by*

$$\begin{aligned} \mathscr{A}_h(u, v) := & \sum_{K \in \mathscr{T}} \int_K \nabla_h u \cdot \nabla_h v \, dx \\ & - \sum_{\gamma \in \mathscr{E}_I \cup \mathscr{E}_D} \int_\gamma \left([\![v]\!] \cdot \{\!\{ \nabla_h u \}\!\} + [\![u]\!] \cdot \{\!\{ \nabla_h v \}\!\} \right) ds \\ & + \sum_{\gamma \in \mathscr{E}_I \cup \mathscr{E}_D} \int_\gamma \sigma \, [\![u]\!] \cdot [\![v]\!] \, ds, \end{aligned} \tag{14}$$

and the corresponding linear functional l_h by

$$l_h(v) := \sum_{K\in\mathscr{T}} \int_K f v \,dx + \int_{\Gamma_N} g v \,ds - \sum_{\gamma\in\mathscr{E}_D} \int_\gamma (\nabla_h v \cdot \vec{n}_\Omega) u_D \,ds + \sum_{\gamma\in\mathscr{E}_D} \frac{\sigma}{|\gamma|} \int_\gamma u_D v \,ds, \tag{15}$$

where $\sigma := C_\sigma 1/h > 0$ is the, so called, discontinuity penalisation parameter. The constant $C_\sigma > 0$ is typically chosen large enough so as to achieve coercivity.

Then, the SIP-dG method of the Poisson problem (4) reads as: Find $u_h \in \mathbb{V}$ such that

$$\mathscr{A}_h(u_h, v_h) = l_h(v_h) \qquad \forall\, v_h \in \mathbb{V}. \tag{16}$$

Some basic properties of the SIP-dG method, such as existence and uniqueness of the result, have been proved in [Wih03]. In particular, we are interested in the subsequent analysis to the following proposition:

Proposition 6 (Consistency of the SIP-dG method) *For $f \in \mathrm{H}^{0,0}_{\vec{\beta}}(\Omega), u_D \in \mathrm{H}^{3/2,3/2}_{\vec{\beta}}(\Gamma_D), g \in \mathrm{H}^{1/2,1/2}_{\vec{\beta}}(\Gamma_N)$, the bilinear form and the linear functional in Definition 2.1 are well-defined and the SIP-dG method is consistent:*

$$\mathscr{A}_h(u, v_h) - l_h(v_h) = 0 \qquad \forall\, v_h \in \mathbb{V}, \tag{17}$$

where $u \in \mathrm{H}^{2,2}_{\vec{\beta}}(\Omega)$ is the exact solution of (4)*. Let $e = u - u_h$ be the error in the SIP-dG method. Using the previous result the following Galerkin orthogonality holds:*

$$\mathscr{A}_h(e, v_h) = 0 \qquad \forall\, v_h \in \mathbb{V}. \tag{18}$$

3 A-posteriori error estimate of the SIP-dG method

In this section, we derive the a-posteriori bound in the L^2 used for both h- and r-adapative strategies in the subsequent numerical experiments.

We consider the dual problem of (4):

$$\begin{aligned} -\Delta\phi &= e \text{ in } \Omega \\ \phi &= 0 \text{ on } \Gamma. \end{aligned} \tag{19}$$

Since $e \in \mathbb{V} \subset \mathrm{H}^{0,0}_{\vec{\beta}}(\Omega)$, the conditions of Theorem 2 are satisfied and the problem (19) admits a (weak) solution $\phi \in \mathrm{H}^{2,2}_{\vec{\beta}}(\Omega)$. Moreover

$$\mathscr{A}_h(\phi, v_h) = l_h(v_h) = \langle e, v_h\rangle_{\mathrm{L}^2(\Omega)} \qquad \forall\, v_h \in \mathbb{V}, \tag{20}$$

where $\langle\cdot,\cdot\rangle_{\mathrm{L}^2(\Omega)}$ on right hand side (rhs) denotes the standard inner product in $\mathrm{L}^2(\Omega)$. This can be used for the derivation of general goal oriented estimators, which can affect the properties of the resulting adapted mesh. We now state the following proposition and lemmas, that will be used for the derivation of the L^2 a-posteriori error estimator:

Proposition 7 (Regularity of the solution on weighted Sobolev Spaces) *Due to Theorem 2.1 [BG88], if $e \in \mathrm{H}^{k,0}_{\vec{\beta}}(\Omega)$, for $k \geq 0$, there exists $\phi \in \mathrm{H}^{k+2,2}_{\vec{\beta}}(\Omega)$, where $\vec{\beta}$ depends on the opening angles at the vertices of Ω, such that*

$$\|\phi\|_{\mathrm{H}^{k+2,2}_{\vec{\beta}}(\Omega)} \leq C(k) \|e\|_{\mathrm{H}^{k,0}_{\vec{\beta}}(\Omega)}. \tag{21}$$

Since $e \in \mathbb{V} \subset \mathrm{H}^{2,2}_{\vec{\beta}}(\Omega)$, we can take $k = 0$ and exploit Remark (1) to obtain

$$\|\phi\|_{\mathrm{H}^{2,2}_{\vec{\beta}}(\Omega)} \leq C \|e\|_{\mathrm{L}^2(\Omega)}. \tag{22}$$

Lemma 8 (Nodal interpolants for dG-FEM) *For an element $K \in \mathscr{T}/\mathscr{K}_0$, let $\Pi_K : \mathscr{C}^0(\overline{K}) \to \mathscr{P}^1(K)$ denote the piece-wise linear operator into polynomials of degree at most one. By standard interpolation results [BS08] there holds*

$$\|v - \Pi_K v\|_{\mathrm{L}^2(K)} \leq C h_K \, \|v\|_{\mathrm{H}^1(K)} \,. \tag{23}$$

In corner elements $K \in \mathscr{K}_0$, the interpolation bounds in [Wih03; Sch98] (Lemma 2.5.3.) for the linear interpolant in the weighted space $\mathrm{H}^{2,2}_{\vec{\beta}}(K)$ for $\beta_K \in [0,1)$ gives

$$\|v - \Pi_K v\|_{\mathrm{H}^1(K)} \leq C h_K^{1-\beta_K} \, \|v\|_{\mathrm{H}^{2,2}_{\beta_k}(K)} \,. \tag{24}$$

Lemma 9 (Discrete trace inequality [EG21]) *Assuming that $P \subset \mathrm{L}^\infty(K)$, there exists a constant c such that the following holds:*

$$\|v\|_{\mathrm{L}^p(F,\mathbb{R}^n)} \leq c \, h_K^{-\frac{1}{p}+n(\frac{1}{p}-\frac{1}{r})} \, \|v\|_{\mathrm{L}^r(K,\mathbb{R}^n)} \,, \tag{25}$$

for all $p, r \in [1,\infty]$, all $v \in P_K$, all $K \in \mathscr{T}$, and all the faces F of K.

We can now proceed with the derivation of the estimator. We start by taking $v_h = e$ in equation (20) and exploit the Galerkin orthogonality for the linear interpolant $\Pi_h v$, defined as $\Pi_h v|_K = \Pi_K v$. We have that $\Pi_K v \subset \mathscr{C}^0(K) \subset \mathbb{V}$. Then, using the Galerkin orthogonality (18)

$$\begin{aligned} \|e\|^2_{\mathrm{L}^2(\Omega)} = \mathscr{A}_h(\phi, e) = \mathscr{A}_h(\phi - \Pi_h\phi, e) = \sum_{K\in\mathscr{T}} \int_K \nabla_h(\phi - \Pi_h\phi) \cdot \nabla_h e \,\dot{x} \\ - \sum_{\gamma\in\mathscr{E}_I} \int_\gamma \big([\![\phi - \Pi_h\phi]\!] \cdot \{\!\{ \nabla_h e \}\!\} + [\![e]\!] \cdot \{\!\{ \nabla_h(\phi - \Pi_h\phi) \}\!\} \big) \dot{s}. \end{aligned} \tag{26}$$

Integration by parts of the first term on the rhs gives

$$\begin{aligned} \|e\|^2_{\mathrm{L}^2(\Omega)} = \sum_{K\in\mathscr{T}} \int_K (\phi - \Pi_h\phi)(f + \Delta_h u_h) \dot{x} \\ + \sum_{\gamma\in\mathscr{E}_I} \int_\gamma \Big((\phi - \Pi_h\phi) \, [\![\nabla_h u_h]\!] + [\![u_h]\!] \cdot \{\!\{ \nabla_h(\phi - \Pi_h\phi) \}\!\} \Big) \dot{s}, \end{aligned}$$

where we have also exploited Remark 1 and Lemma 5 on u and $\nabla_h u$, respectively.
We then apply the Cauchy-Schwartz inequality:

$$\begin{aligned} \|e\|^2_{\mathrm{L}^2(\Omega)} \leq \sum_{K\in\mathscr{K}_0} \|\phi - \Pi_h\phi\|_{\mathrm{L}^2(K)} \, \|f + \Delta_h u_h\|_{\mathrm{L}^2(K)} + \sum_{K\in\mathscr{T}/\mathscr{K}_0} \|\phi - \Pi_h\phi\|_{\mathrm{L}^2(K)} \, \|f + \Delta_h u_h\|_{\mathrm{L}^2(K)} \\ + \sum_{\gamma\in\mathscr{E}_I} \|\phi - \Pi_h\phi\|_{\mathrm{L}^2(\gamma)} \, \|[\![\nabla_h u_h]\!]\|_{\mathrm{L}^2(\gamma)} + \sum_{\gamma\in\mathscr{E}_I} \|[\![u_h]\!]\|_{\mathrm{L}^2(\gamma)} \, \|\nabla_h \{\!\{ \phi - \Pi_h\phi \}\!\}\|_{\mathrm{L}^2(\gamma)} \,. \end{aligned} \tag{27}$$

For the first term we have by Lemma 8 and Proposition 7 that

$$\|\phi - \Pi_h\phi\|_{\mathrm{L}^2(K)} \leq C h_K \, \|\phi - \Pi_h\phi\|_{\mathrm{H}^1(K)} \leq C h_K^{2-\beta_K} \, |\phi|_{\mathrm{H}^{2,2}_{\vec{\beta}}(\Omega)} \leq C h_K^{2-\beta_K} \, \|e\|_{\mathrm{L}^2(\Omega)} \qquad \forall\, K \in \mathscr{K}_0. \tag{28}$$

For the second term, Lemma 8 gives

$$\|\phi - \Pi_h\phi\|_{\mathrm{L}^2(K)} \leq C h_K^2 \, |\phi|_{\mathrm{H}^2(K)} \leq C h_K^2 \, \|e\|_{\mathrm{L}^2(\Omega)} \qquad \forall\, K \in \mathscr{T}/\mathscr{K}_0. \tag{29}$$

For the remaining two terms we have:

$$\|\phi - \Pi_K\phi\|_{L^2(\gamma)} \leq C\sqrt{h_K}\,\|\phi - \Pi_K\phi\|_{\mathrm{H}^1(K)}$$
$$\leq \begin{cases} Ch_K^{3/2-\beta_K}\,\|\phi\|_{\mathrm{H}^{2,2}_{\beta_K}(K)} \leq Ch_K^{3/2-\beta_K}\,\|e\|_{\mathrm{L}^2(\Omega)} & \text{if } \gamma \in K \in \mathscr{K}_0, \\ Ch_K^{3/2}\,\|\phi\|_{\mathrm{H}^2(K)} \leq Ch_K^{3/2}\,\|e\|_{\mathrm{L}^2(\Omega)} & \text{if } \gamma \in K \notin \mathscr{K}_0. \end{cases} \tag{30}$$

Using Lemma 9 we obtain the upper bound:

$$\begin{aligned} \|\{\!\{\ \nabla_h(\phi - \Pi_K\phi)\ \}\!\}\|_{\mathrm{L}^2(\gamma)} &\leq Ch_K^{-1/2}\,\|\nabla_h(\phi - \Pi_K\phi)\|_{\mathrm{L}^2(K)} \\ &\leq h_k^{-1/2}\,\|\phi - \Pi_K\phi\|_{\mathrm{H}^1(K)} \\ &\leq \begin{cases} Ch_k^{1/2-\beta_k}\,\|e\|_{L^2(\Omega)} & \text{if } \gamma \in K \in \mathscr{K}_0, \\ Ch_k^{1/2}\,\|e\|_{^2(\Omega)} & \text{if } \gamma \in K \notin \mathscr{K}_0. \end{cases} \end{aligned} \tag{31}$$

Replacing the results obtained in (28)-(31) in equation (27) we have:

$$\begin{aligned} \|e\|_{\mathrm{L}^2(\Omega)} \leq C_1 \sum_{K\in\mathscr{K}_0} \Bigg(& h_K^{2-\beta_K}\,\|f + \Delta_h u_h\|_{\mathrm{L}^2(K)} + \\ & \frac{1}{2}\sum_{\partial K\in\mathscr{E}(K)} \left(h_K^{3/2-\beta_K}\,\|\nabla_h u_h\|_{\mathrm{L}^2(\partial K)} + h_K^{1/2-\beta_K}\,\|u_h\|_{\mathrm{L}^2(\partial K)}\right)\Bigg) \\ & + C_2 \sum_{K\in\mathscr{T}/\mathscr{K}_0} \Bigg(h_K^2\,\|f + \Delta_h u_h\|_{\mathrm{L}^2(K)} + \frac{1}{2}\sum_{\partial K\in\mathscr{E}(K)} \left(h_K^{3/2}\,\|\nabla_h u_h\|_{\mathrm{L}^2(\partial K)} + h_K^{1/2}\,\|u_h\|_{\mathrm{L}^2(\partial K)}\right)\Bigg). \end{aligned} \tag{32}$$

This expression can be simplified if $u \in \mathbb{V}$ with $p = 1$ and $f = 0$. We further introduce the indicator function $1_{\gamma\in\mathscr{E}_I(\mathscr{K}_0)}$ and rewrite (32) in the more compact form

$$\begin{aligned} \|e\|_{\mathrm{L}^2(\Omega)} &\leq \sum_{\gamma\in\mathscr{E}_I} \left(h_{K(\gamma)}^{3/2-1_{\gamma\in\mathscr{E}_I(\mathscr{K}_0)}\beta_\gamma}\,\|[\![\nabla_h u_h]\!]\|_{\mathrm{L}^2(\gamma)} + h_{K(\gamma)}^{1/2-1_{\gamma\in\mathscr{E}_I(\mathscr{K}_0)}\beta_\gamma}\,\|[\![u_h]\!]\|_{\mathrm{L}^2(\gamma)}\right) \\ &\leq \left(\sum_{\gamma\in\mathscr{E}_I} h_{K(\gamma)}^{3-1_{\gamma\in\mathscr{E}_I(\mathscr{K}_0)}2\beta_\gamma}\,\|[\![\nabla_h u_h]\!]\|^2_{\mathrm{L}^2(\gamma)} + h_{K(\gamma)}^{1-1_{\gamma\in\mathscr{E}_I(\mathscr{K}_0)}2\beta_\gamma}\,\|[\![u_h]\!]\|^2_{\mathrm{L}^2(\gamma)}\right)^{1/2}. \end{aligned} \tag{33}$$

For practical purposes, we reformulate (33) for each K in order to obtain a cell-wise error indicator:

$$\|e\|^2_{\mathrm{L}^2(\Omega)} \leq \sum_{K\in\mathscr{T}} \sum_{\gamma\in\mathscr{E}_I(K)} h_K^{3-1_{\gamma\in\mathscr{E}_I(\mathscr{K}_0)}2\hat{\beta}_\gamma}\,\|[\![\nabla_h u_h]\!]\|^2_{\mathrm{L}^2(\gamma)} + h_K^{1-1_{\gamma\in\mathscr{E}_I(\mathscr{K}_0)}2\hat{\beta}_\gamma}\,\|[\![u_h]\!]\|^2_{\mathrm{L}^2(\gamma)}, \tag{34}$$

where $\hat{\beta} \in [0,1]$ replaces the weight β, whose range is specified in Remark 3. Here, actually, $\hat{\beta}$ defines an upper bound for the L^2 error and does not prevent the solution u of problem 4 to lie in an admissible weighted Sobolev space.

We conclude this section by presenting an L^∞ a-posteriori estimator for the SIP-dG method [DG12] . The domain Ω is not required to be Lipschitz, thus the following bound can be tested for our numerical experiments:

$$\|u - u_h\|_{\mathrm{L}^\infty(\Omega)} \leq Cl_{h,d}\Big(\left\|h^2(f + \Delta_h u_h)\right\|_{\mathrm{L}^\infty(\Omega)} + \|h\,[\![\nabla u_h]\!]\|_{\mathrm{L}^\infty(\mathscr{E}_I)} + \|[\![u_h]\!]\|_{\mathrm{L}^\infty(\mathscr{E}_I)} + \|u_D - u_h\|_{\mathrm{L}^\infty(\partial\Omega)}\Big), \tag{35}$$

where $l_{h,d} = (\ln 1/\underline{h})^2$.

4 Numerical Results

In this section we consider as model problem the Poisson equation

$$\begin{aligned} -\Delta u &= 0 \text{ in } \Omega \\ u_D(r,\theta) &= r^{\pi/\omega} sin\,(\pi\theta/\omega) \text{ on } \Gamma, \end{aligned} \tag{36}$$

where $\omega \in (\pi, 2\pi)$ is the angle of the re-entrant corner located at $\vec{0} = (0,0) \in \mathbb{R}^2$. We evidence that u is analytic in $\overline{\Omega}/\{\vec{0}\}$ and $u \notin \mathrm{H}^2(\Omega)$, so that $SP(\Omega, \Gamma_D, \Gamma_N) = \{A_1 := \vec{0}\}$. Therefore, the weight function is defined as $\Phi_\beta(\vec{x}) = |\vec{x}|^\beta$, where $\beta \in (1 - \frac{\pi}{\omega}, 1]$, according to Remark 3. Let Ω be the L-shaped domain $(-1,1)^2/[0,1) \times (-1,0]$. Then, the harmonic solution of problem (36) is

$$u(r,\theta) = r^{2/3} sin(2\theta/3). \tag{37}$$

We compare the accuracy of the SIP-dG method applied to problem (36) using different adaptive mesh strategies and assess the quality of the resulting meshes. For all the tests, we compute the numerical solution $u_h \in \mathbb{V}$ with $p = 1$. All the tests have been performed in FEniCS [LW10].

4.1 h-refinement

In the h- adaptive process, we introduce the global error indicator $\eta^2 = \sum_{K \in \mathscr{T}} \eta_K^2$, where η_K^2 refers to each cell K on the rhs of equation (34). As a widely accepted criterion, elements with large error estimator should be marked for refinement. Here, we employ the so called *maximum strategy* (*ms*). The same procedure is applied for the L^∞ a-posteriori bound, denoted by $\tilde{\eta_K}$.

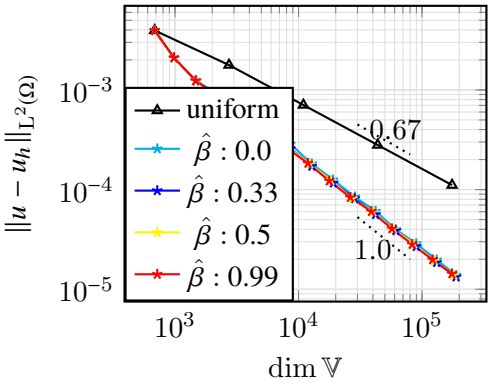

Figure 1: Asymptotic convergence rates for the h-refinement strategy on the finite element space $\mathbb{V}$. Note that the rate of convergence is optimal and independent on $\hat{\beta}$. Uniform mesh refinement yields a convergence rate of $2/3$ due to the singular behaviour of the solution near the origin [GMP17].

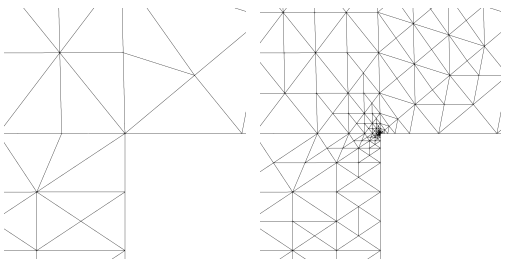

(a) $\hat{\beta} = 0.0$. (b) $\hat{\beta} = 0.99$.

Figure 2: Mesh obtained via the L^2 a-posteriori bound (34) after 15 refinements.

The *ms* h-refinement strategy with has been tested for different $\hat{\beta}$. We observe that the level of refinement is increasing near the corner as a function of $\hat{\beta}$ (Fig. 2) but does not affect the order of convergence (Fig. 1).

4.2 r-adaptive strategy

The r-adaptive strategy aims to generate an adapted mesh $\mathscr{T}$ by relocating a fixed number of mesh points. This process can be interpreted as the image from a computational domain Ω_c, having a fixed mesh $\mathscr{T}_c$, to a physical domain Ω with mesh $\mathscr{T}$. An adaptive mesh based on *Optimal Transport* will be constructed by considering the strong dependence of the solution on the radial variable and not on the angular one, which results in a one-dimensional non-algebraic equation, easily solvable via the relaxed Newton–Raphson method. For an in-depth survey of other r-adaptive strategies, we refer the reader to [BHR09].

4.2.1 Optimal Transport mesh

We devise a mesh for the L-shaped region by solving the Monge-Ampère equation close to the re-entrant corner. The solution is then tuned to match the boundary of the domain.

Local mesh scaling Consider the general solution of equation (36). We know that the interpolation error of the solution for piecewise linear element can be bounded in the L^2 norm by $E_{max} \sim h^2 r^{\pi/\omega-2}$, where h is the local mesh size of an element close to the corner and r is the distance from the re-entrant corner, placed at the origin of $\mathbb{R}^2$.

Following the *equidistribution principle*, we impose $E_{max} = 1$, so that we obtain $h \sim r^{\gamma}$, where $\gamma = 1 - \frac{\pi}{2\omega}$. Given the computation variable s, which represent the distance from the origin in the computational domain $\Omega_c \equiv \Omega$, we can interpret h as being proportional to dr/ds. Solving the differential equation $\frac{dr}{ds} = h = r^{\gamma}$ we obtain that $r \sim s^{\frac{1}{1-\gamma}}$.

Solution of Monge-Ampère equation We now look for a radially symmetric transformation from the corner region to itself. We can assume a radial symmetry because the singular behaviour of the solution near the origin does not depend on the angle θ. More details on the application of approach can be found in [BRW15]. Locally, the first integral of the Monge-Ampère equation implies that r satisfies the Ordinary Differential Equation (ODE) in polar coordinates

$$m(r) r \, dr d\theta = s \, ds d\theta, \tag{38}$$

where $m(r) = r^{-2\gamma}$ is the monitor function, which will be determined by the *a-priori* estimate for the interpolation error.

We expect that for large r the adapted mesh is almost regular. we then expect that $m(r) \sim 1$ far from the corner and consider the general expression

$$m(r) = A + B r^{-2\gamma}, \quad \alpha, \beta \in \mathbb{R} \tag{39}$$

From (38) we integrate over the variable θ and obtain

$$\left(A + B r^{-2\gamma}\right) r \frac{dr}{ds} = s,$$

so that r satisfies the nonlinear algebraic equation

$$A r^2 + \frac{B}{1-\gamma} r^{2(1-\gamma)} = s^2. \tag{40}$$

The equation (40) then determines the mesh transformation. Note that the parameter A and B controls the level of mesh compression near the corner. In fact, for high values of B and small r we have $r \sim s^{1/(1-\gamma)}$ and for large A and r we have $r \sim s$. For the remainder of the analysis, we choose $B = (1-\gamma)$, as this is the maximum admissible value that respects the boundary condition $A + B/(1-\gamma) = 1$ when $r, s = 1$.

Computation of the OT mesh Suppose we have a uniform regular mesh $(\xi_{i,j}, \eta_{i,j})$ in Ω_c which we want to map to an adapted non uniform mesh $(x_{i,j}, y_{i,j})$ in the physical domain, with $i, j = 1, \dots, N$. The application of the Monge-Ampère method provides the desired mesh as follows:

1. For each pair (i, j) compute $s_{i,j}^2 = \xi_{i,j}^2 + \eta_{i,j}^2$
2. Compute the angle $\theta_{i,j}$ with respect to the semi-positive x axis by $\arctan\left(\frac{\eta_{i,j}}{\xi_{i,j}}\right)$.
3. Compute the length $l_{i,j}$ of the line spanned from the origin with angle $\theta_{i,j}$ to the boundary of the L-shaped domain.
4. Set the parameter $B = 1 - \gamma$ and enforce the condition $A + \frac{B}{1-\gamma} l_{i,j}^{-2\gamma} = 1$. This ensures that the new mesh boundary matches with the original boundary region.
5. Solve equation (40) to find $r_{i,j}$
6. Set $(x_{i,j}, y_{i,j}) = \frac{r_{i,j}}{s_{i,j}}(\xi_{i,j}, \eta_{i,j})$.

Given the new mesh $(x_{i,j}, y_{i,j})$, we can increase the resolution by applying the previous procedure from a more graded uniform mesh.

OT mesh for different γ In this Section, we show how the parameter γ affects the accuracy and the quality of the resulting OT mesh. The theoretical derivation of the optimal values is provided in the Appendix (6).

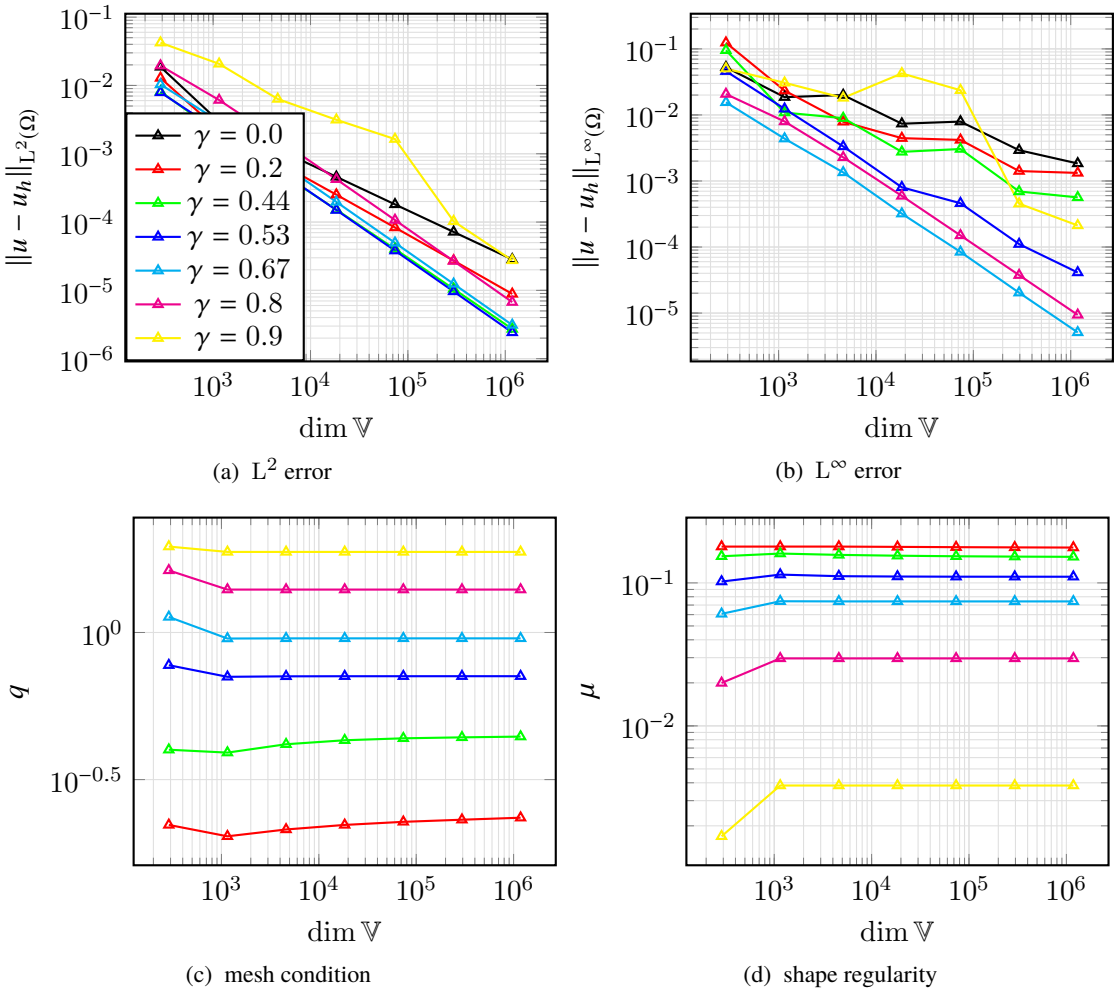

(a) L^2 error (b) L^∞ error

(c) mesh condition (d) shape regularity

Figure 3: Error and quality measure of the OT mesh for different γ.

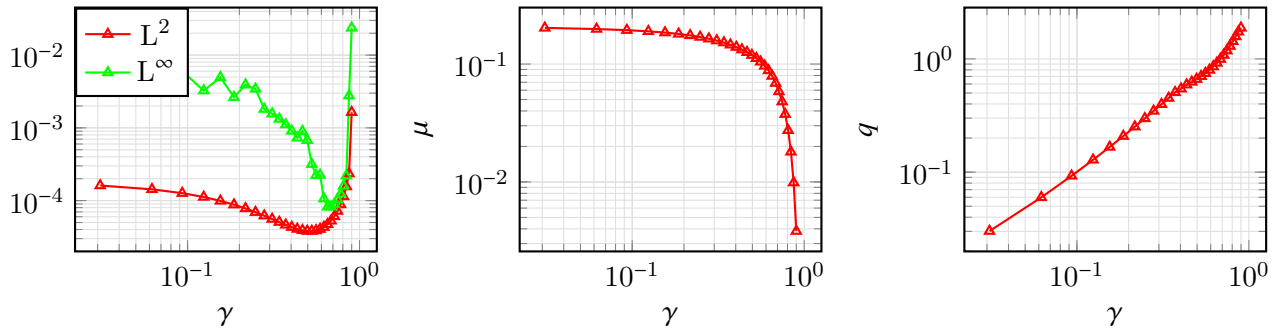

(a) Error (b) Shape regularity (c) Mesh condition

Figure 4: Error and quality measures for the a-priori OT mesh as function of γ ($\dim \mathbb{V} = 73728$).

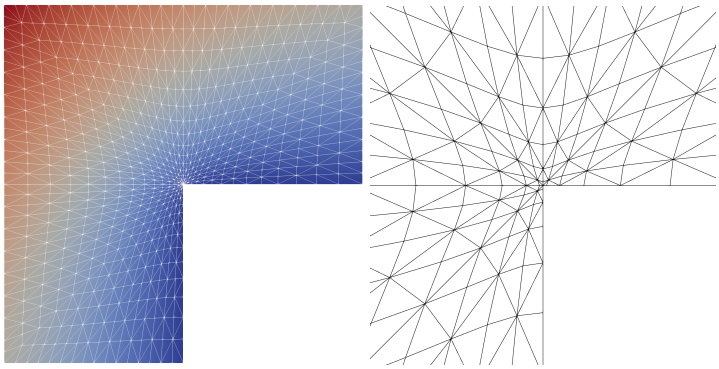

Figure 5: (Left) Solution of eq.(36) on the OT mesh with $\gamma = 0.53$. (Right) Zoom of the OT mesh on the re-entrant corner.

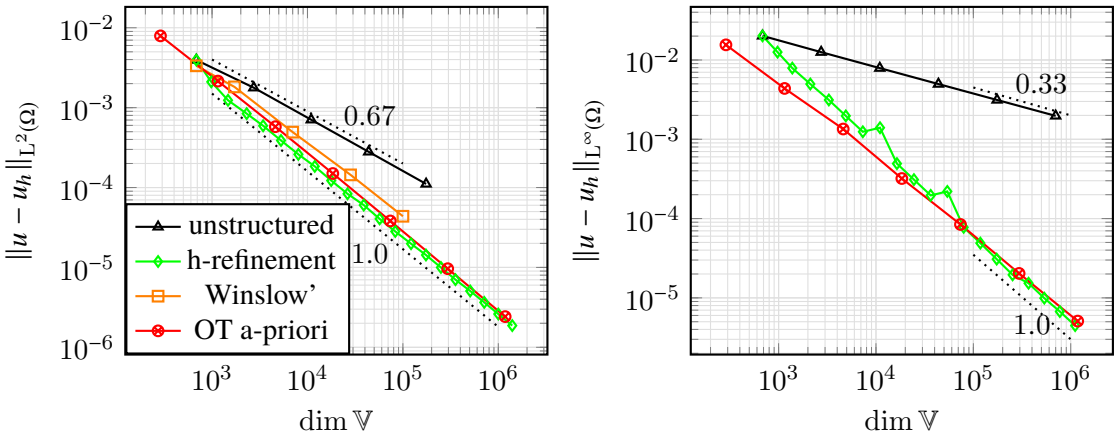

(a) L^2 error (b) L^∞ error

Figure 6: Asymptotic convergence rates for different adaptive strategies. Note that the rate of convergence is optimal for h-refinement and the OT strategy ($\gamma = 0.53, 0.67$ for L^2 and L^∞ norm, respectively).

Link between OT mesh and a-posteriori measure In this section we analyse the relationship between the a-posteriori bound η_K used for h-adaptivity and the OT mesh obtained previously.

We first remark that purpose of h-refinement is to equidistribute η_K throughout each cell by reducing the element mesh size through bisection. The result leads to the minimisazion of the overall truncation error. We then expect that the optimal γ obtained in the Appendix (6) is also able to equidistribute η_K in the vicinity of the origin. Indeed, the γ achieving the highest accuracy is the best in equidistributing 6a and 6b.

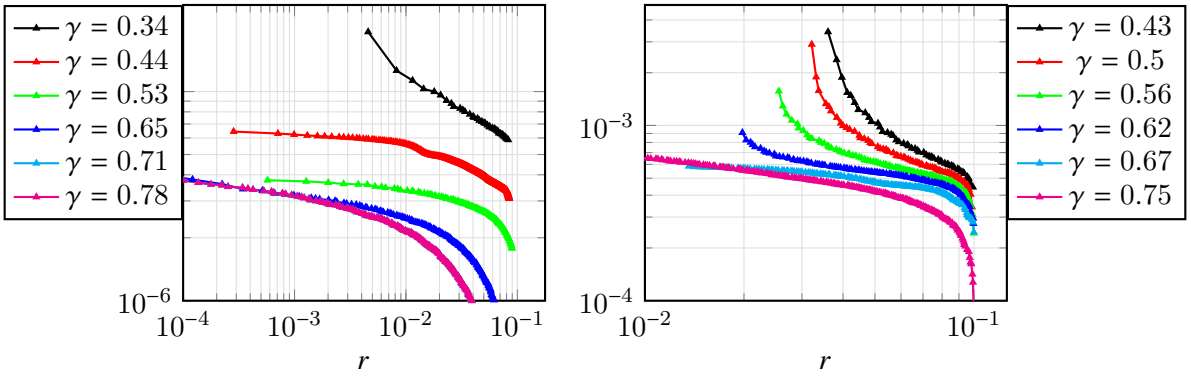

(a) L^2 norm (b) L^∞ norm

Figure 7: Cell values of the a-posteriori measure η_K for OT meshes with $\dim \mathbb{V} = 7 \times 10^4$ for different values of γ. The measure has been computed as a function of the distance from the re-entrant corner.

4.3 Crack domain

Let Ω be the domain with a crack $(-1,1) \times (1,1)/([(0,1) \times \{0\}])$. The solution of Equation 36 is

$$u(r,\theta) = r^{1/2} sin(\theta/2) \tag{41}$$

Numerically, the interior angle ω has been set to $2\pi - \epsilon$, with $\epsilon = 10^{-3}$.

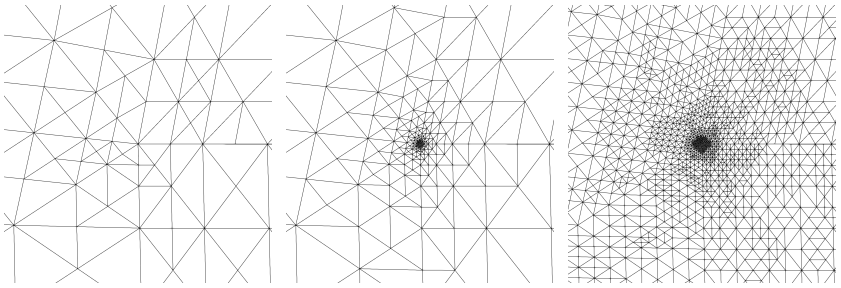

(a) L^2 a-posteriori ($\beta = 0.0$) (b) L^2 a-posteriori ($\beta = 0.99$) (c) L^∞ a-posteriori bound

Figure 8: Zoom of the mesh near the re-entrant corner obtained with the a-posteriori bounds (34)-(35).

OT mesh for different γ In this Section, we show how the parameter γ, introduced in 4.2.1, affects the accuracy and the quality of the resulting OT mesh. The theoretical derivation of the optimal values is provided in the Appendix (6).

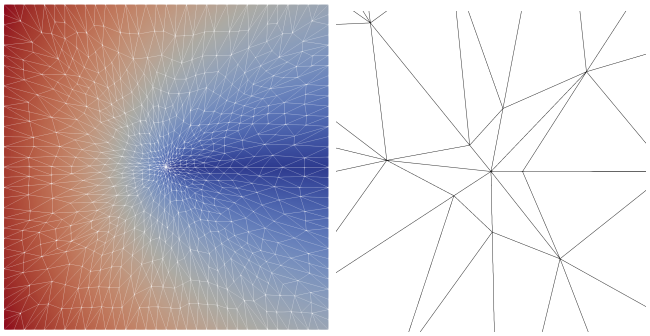

Figure 9: (Left) Solution of the Poisson eq. 41. (Right) Zoom of the OT mesh near the origin.

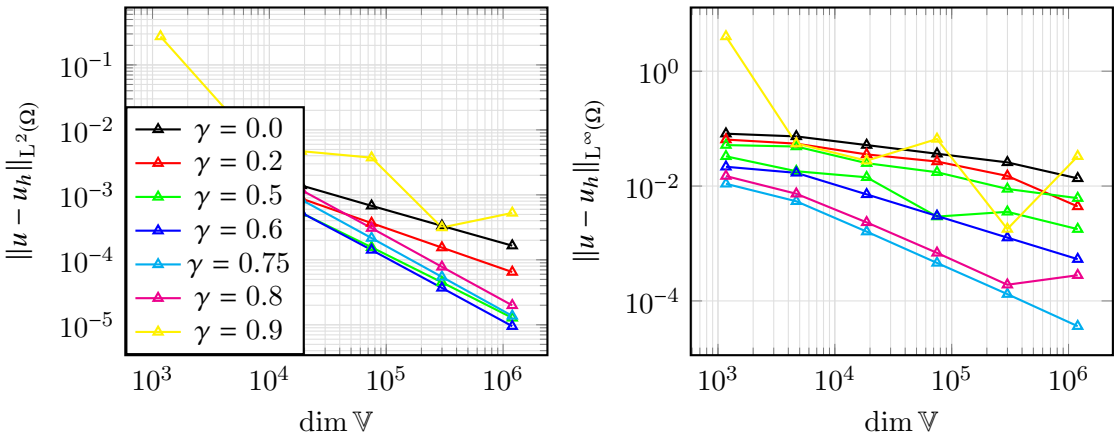

(a) L^2 error

(b) L^∞ error

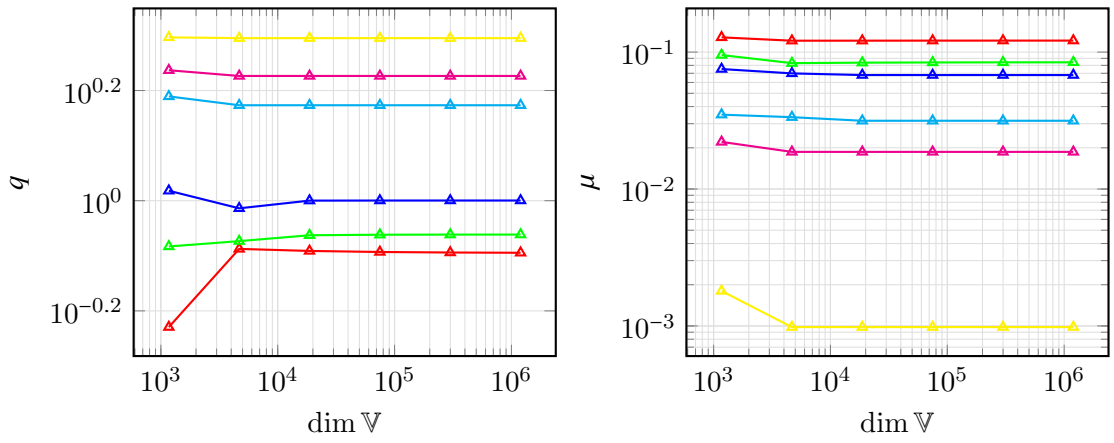

(c) mesh condition

(d) shape regularity

Figure 10: Error and quality measure for OT mesh for different γ.

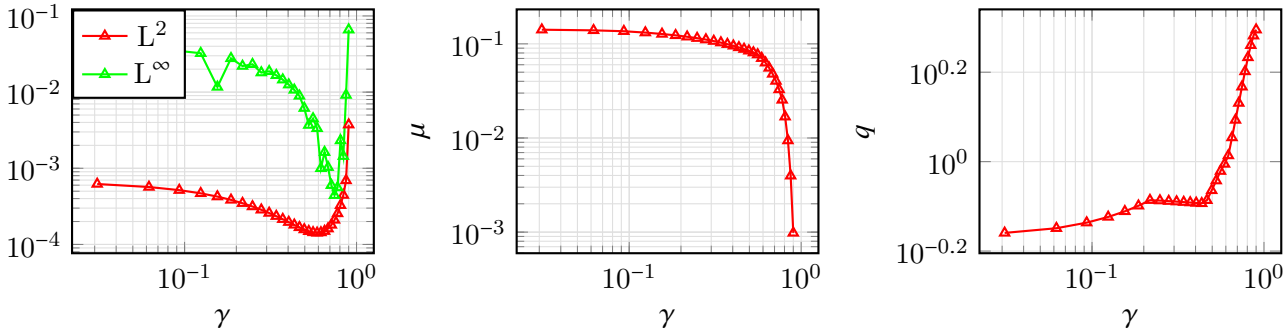

(a) Error (b) Shape regularity (c) Mesh condition

Figure 11: Error and quality measures for the a-priori OT mesh as function of γ ($\dim \mathbb{V} = 74880$).

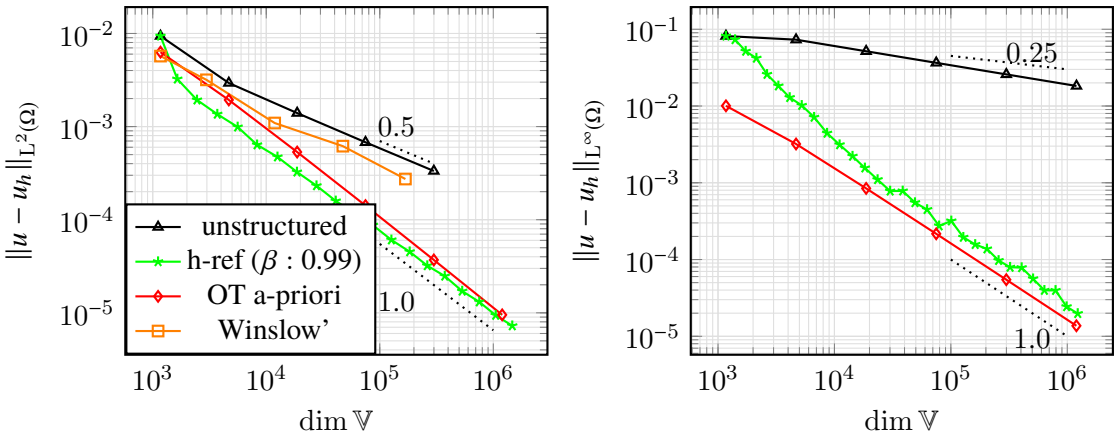

(a) L^2 error (b) L^∞ error

Figure 12: Asymptotic convergence rates for different adaptive strategies. Note that the rate of convergence is optimal for h-refinement and the OT strategy ($\gamma = 0.6, 0.75$ for L^2 and L^∞ norm, respectively).

Link between OT mesh and a-posteriori measure In this section, we investigate the relationship between the a-posteriori bound η_K and the OT mesh as done for the L-shaped domain. The plots below evidence again that the a-posteriori estimator is equidistributed near the origin for the value of γ providing the highest accuracy.

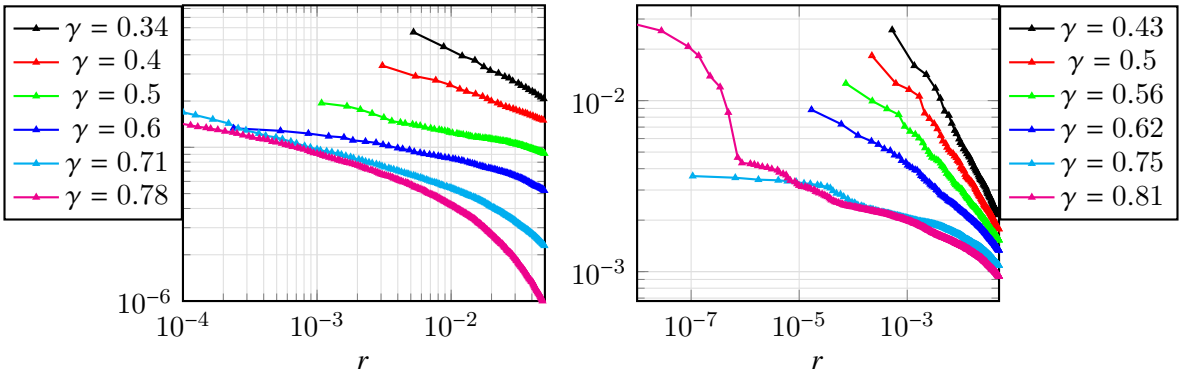

(a) L^2 norm (b) L^∞ norm

Figure 13: Cell values of the a-posteriori measure η_K for OT meshes with $\dim \mathbb{V} = 7 \times 10^4$ for different values of γ. The measure has been computed as a function of the distance from the re-entrant corner.

5 Mesh Skewness

The quality of the OT mesh can be expressed in terms of different measures. Besides the shape regularity and mesh condition, a common metric used in the context of r-adaptive methods is the *skewness*, which indicates how far mesh elements are from being equilateral. A general indicator for triangular elements has been proposed in [BHR09] and employs the local map $Q_K : \widehat{K} \to K$, with $\widehat{K} \in \mathscr{T}_c$ and $K \in \mathscr{T}$. Given the corresponding Jacobian $\boldsymbol{J}_K$ with eigenvalues λ_1 and λ_2, the quality measure for the element K is defined as

$$Q_K := \frac{1}{2}\left(\frac{\lambda_1}{\lambda_2} + \frac{\lambda_2}{\lambda_1}\right). \tag{42}$$

We define the *global quality measure* as

$$Q = \max_{K \in \mathscr{T}} Q_K \tag{43}$$

Under the OT transformation $(x, y) = \frac{r}{s}(\xi, \eta)$, we can determine the value of Q analytically. As the mesh gets more uniform away from the corner, we assume that Q is given for cells where $r \sim 0$, so that the algebraic expression (40) simplifies to $r^{1-\gamma} = s$. We then compute the Jacobian of the map $(x, y) = s^{\frac{\gamma}{1-\gamma}}(\xi, \eta)$:

$$\boldsymbol{J} = \begin{bmatrix} x_\xi & x_\eta \\ y_\xi & y_\eta \end{bmatrix} = \frac{\gamma}{1-\gamma}(\xi^2 + \eta^2)^{\frac{\gamma}{2(1-\gamma)}-1} \begin{bmatrix} \xi^2 + (\xi^2+\eta^2)^{\frac{1-\gamma}{\gamma}} & \xi\eta \\ \xi\eta & \eta^2 + (\xi^2+\eta^2)^{\frac{1-\gamma}{\gamma}}. \end{bmatrix}$$

The eigenvalues are $\lambda_1 = \frac{1-\gamma}{\gamma}(\xi + \nu)^2$ and $\lambda_2 = \frac{1}{\gamma}(\xi + \nu)^2$. Finally, the skewness is expressed in terms of the coefficient γ by:

$$Q(\gamma) = \frac{1}{2}\left(\frac{\lambda_1}{\lambda_2} + \frac{\lambda_2}{\lambda_1}\right) = \frac{1}{2}\left((1-\gamma) + \frac{1}{(1-\gamma)}\right). \tag{44}$$

This shows that as γ increases, the mesh quality deteriorates. This is also qualitatively suggested by looking at the OT mesh produced for the L-shaped and the crack domain (5)-(9).

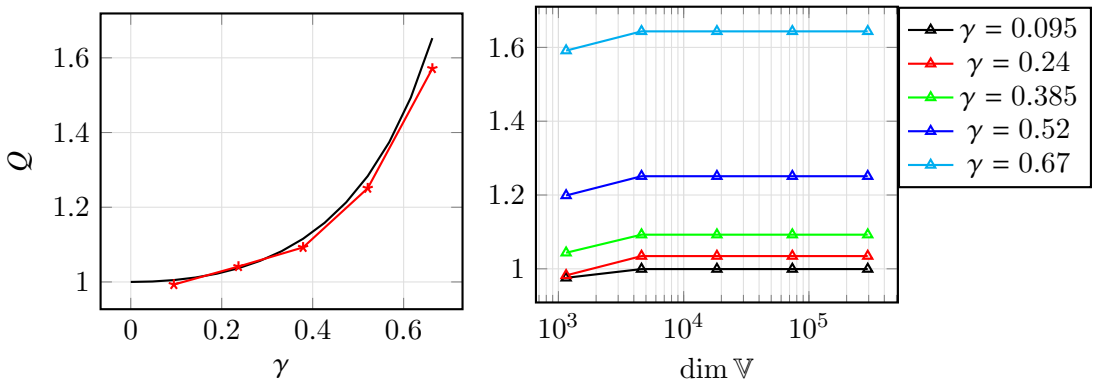

(a) Skewness of OT mesh as a function of γ (b) Skewness of OT mesh as a function of $\dim \mathbb{V}$

Figure 14: (Left) We show that the dependence of the skewness measure on γ computed numerically fits the theoretical formula in (44). (Right) The value of $Q(\gamma)$ is independent on the dimension of the FE space.

6 Conclusions

In this paper, we have analysed the relationship between h-adaptive and an OT based strategy for the solution of the Poisson equation on the L-shaped and crack domain. We first derived the SIP-dG variational formulation using the framework of weighted Sobolev spaces. This has allowed us to derive an L^2 a-posteriori error estimate. An L^∞ estimator has also been adopted for h-refinement and both achieve optimal order of convergence.

As r-adaptive method, we have constructed an *Optimal Transport* based mesh, which accounts for the singular behaviour of the solution near the re-entrant corner. As this does mainly depend on the radial variable, it is possible to formulate the OT problem in one-dimension and avoid the numerical treatment of the more demanding two-dimensional Monge-Ampère equation. The optimality of the convergence rate and accuracy with the proposed approach requires the specification of a hyper-parameter, which controls the level of node clustering close to the origin. The critical value has been derived theoretically using a one-dimensional equidistribution strategy for both L^2 and L^∞ norms. Numerical tests convalidate these findings. Furthermore, the optimally-tuned OT mesh equidistributes the a-posteriori estimates used for the h-refinement. This evidences the close relationship of the two methods and the common goal of minimising the overall truncation error via equidistribution.

Finally, we have introduced the *skewness* as a quality measure for the OT method and have showed both theoretically and numerically that it increases only as a function of the re-entrant angle and is independent on the dimension of the FE space.

In the view of the above considerations, our future research directions will examine:

1. Theoretical proof of the a-poteriori estimator equidistribution for the optimal one-dimensional monitor function used in r-adaptation;
2. Application of the numerical procedure on polygons with multiple re-entrant cornerns and to other relevant time-dependent problems arising in physics, such as the Shallow-Water equations;
3. Investigation on the relationship between different mesh quality measures;
4. Scalability of the OT generation algorithm through parallelisation;
5. Extension of the OT strategy by solving the fully Monge-Ampère type equation [BRW15].

References

[BR72] I. Babŭska and M.B. Rosenzweig. “A Finite Element Scheme for Domains with Corners”. In: *Numer. Math.* 20.1 (1972), pp. 1–21.

[BKP79] I. Babŭska, R.B. Kellogg, and J. Pitkäranta. “Direct and Inverse Error Estimates for Finite Elements with Mesh Refinements”. In: *Numer. Math.* 33.4 (1979), pp. 447–471.

[Arn82] D. Arnold. “An Interior Penalty Finite Element Method with Discontinuous Elements”. In: *SIAM Journal on Numerical Analysis* 19.4 (1982), pp. 742–760.

[BG88] I. Babŭska and B.Q. Guo. “Regularity of the Solution of Elliptic Problems with Piecewise Analytic Data. Part I. Boundary Value Problems for Linear Elliptic Equation of Second Order”. In: *SIAM Journal on Mathematical Analysis* 19.1 (1988), pp. 172–203.

[BG89] I. Babŭska and B. Q. Guo. “Regularity of the Solution of Elliptic Problems with Piecewise Analytic Data. II: The Trace Spaces and Application to the Boundary Value Problems with Nonhomogeneous Boundary Conditions”. In: *SIAM Journal on Mathematical Analysis* 20.4 (1989), pp. 763–781.

[Sch98] C. Schwab. *p-and hp-finite element methods: Theory and applications in solid and fluid mechanics*. Oxford University Press, 1998.

[Arn+00] D. Arnold et al. “Discontinuous Galerkin Methods”. In: vol. 11. 2000, pp. 89–101.

[Arn+02] D. Arnold et al. “Unified Analysis of Discontinuous Galerkin Methods for Elliptic Problems”. In: *SIAM J. Numer. Anal.* 39 (2002).

[ZS02] C. Zhiqiang and K. Seokchan. “A Finite Element Method Using Singular Functions for the Poisson Equation: Corner Singularities”. In: *SIAM Journal on Numerical Analysis* 39.1 (2002), pp. 286–299.

[ZSG02] C. Zhiqiang, K. Seokchan, and W. Gyungsoo. “A finite element method using singular functions for the Poisson equation: crack singularities”. In: *Numerical Linear Algebra with Applications* 9.6-7 (2002), pp. 445–455.

[Wih03] T. Wihler. “Discontinuous Galerkin FEM for elliptic problems in polygonal domains”. PhD thesis. 2003.

[BS08] S.C. Brenner and L.R. Scott. *The Mathematical Theory of Finite Element Methods*. Vol. 15. Texts in Applied Mathematics. Springer, 2008.

[BHR09] C. Budd, W. Huang, and R. Russell. “Adaptivity with moving grids”. In: *Acta Numerica* 18 (2009), pp. 111–241.

[LW10] A. Logg and G.N. Wells. “DOLFIN”. In: *ACM Transactions on Mathematical Software* 37.2 (2010), pp. 1–28.

[HR11] W. Huang and R. Russell. *Adaptive Moving Mesh Methods*. Vol. 174. 2011.

[DG12] A. Demlow and E. H. Georgoulis. “Pointwise a Posteriori Error Control for Discontinuous Galerkin Methods for Elliptic Problems”. In: *SIAM Journal on Numerical Analysis* 50.5 (2012), pp. 2159–2181.

[BRW15] C.J. Budd, R.D. Russell, and E. Walsh. “The geometry of r-adaptive meshes generated using optimal transport methods”. In: *Journal of Computational Physics* 282 (2015), pp. 113–137.

[SH16] K. Seokchan and L. Hyung-Chun. “A finite element method for computing accurate solutions for Poisson equations with corner singularities using the stress intensity factor”. In: *Computers and Mathematics with Applications* 71.11 (2016), pp. 2330–2337.

[GMP17] E. Georgoulis, C. Makridakis, and T. Pryer. "Babŭska-Osborn techniques in discontinuous Galerkin methods: L^2-norm error estimates for unstructured meshes". In: *arXiv:1704.05238* (2017).

[EG21] Alexandre Ern and Jean-Luc Guermond. *Finite Elements I: Approximation and Interpolation*. 2021.

A Derivation of optimal γ for L^∞- and L^2-error norm

A.1 L^∞ norm

We derive here the optimal value of the exponent γ that minimises the L^∞ norm. We consider the function $u(r) = r^\alpha$, where α is a parameter that depends on the interior angle of the re-entrant corner. As $\alpha < 1$ and $u \notin C^2[0,1]$, we must split the error analysis into two parts. Then, we write

$$\left\|u - p_{1,N}\right\|_{\infty,[0,1]} = \max\{\left\|u - p_{1,N}\right\|_{\infty,[0,x_1]}, \left\|u - p_{1,N}\right\|_{\infty,[x_1,1]}\}$$

For the first part, by triangle inequality

$$\left\|u - p_{1,N}\right\|_{\infty,[0,x_1]} \leq \|u\|_{\infty,[0,x_1]} + \left\|p_{1,N}\right\|_{\infty,[0,x_1]} = x_1^\alpha + p_{1,N}(x_1) = 2\left(\left(\frac{1}{N}\right)^\beta\right)^\alpha = 2N^{-\alpha\beta}, \quad (45)$$

using the fact that both u and $p_{1,N}$ is an increasing function.
We treat each interval $[x_{j-1}, x_j]$ for $j \geq 2$ separately. For $h_j = x_j - x_{j-1}$, we have

$$\left\|u - p_{1,N}\right\|_{\infty,[x_{j-1},x_j]} \leq \frac{1}{8}h_j^2 \left\|u''\right\|_{\infty,[x_{j-1},x_j]},$$

with

$$\left\|u''\right\|_{\infty,[x_{j-1},x_j]} = \sup_{[x_{j-1},x_j]} |u''| = |\alpha(\alpha-1)|x_{j-1}^{\alpha-2} = |\alpha(\alpha-1)|\left(\frac{j-1}{N}\right)^{\beta(\alpha-2)}.$$

Using the mean-value theorem for the increasing function $g(t) = t^\beta$ on the interval $t_j \in [(j-1)/N, j/N]$ we have

$$h_j = x_j - x_{j-1} = g(j) - g(j-1) = [j-(j-1)]g'(t_j) = \frac{1}{N}\beta\left(\frac{t_j}{N}\right)^{\beta-1} \leq \frac{\beta}{N}\left(\frac{j}{N}\right)^{\beta-1}.$$

We then obtain

$$\left\|u - p_{1,N}\right\|_{\infty,[x_{j-1},x_j]} \leq \frac{|\alpha(\alpha-1)|}{8}\beta^2 N^{-\alpha\beta}\left(\frac{j^{2(\beta-1)}}{(j-1)^{\beta(2-\alpha)}}\right) \quad (46)$$

Finally, Eqs. (45) and (46) give

$$\left\|u - p_{1,N}\right\|_{\infty,[0,1]} \leq \max_{j=1,\ldots,N}\{\left\|u - p_{1,N}\right\|_{\infty,[x_{j-1},x_j]}\} \leq N^{-\alpha\beta} \max_{j=2,\ldots,N}\left\{2, \frac{|\alpha(\alpha-1)|}{8}\beta^2\frac{j^{2(\beta-1)}}{(j-1)^{\beta(2-\alpha)}}\right\}.$$

By imposing $2(\beta-1) = \beta(2-\alpha) \Rightarrow \beta = 2/\alpha$ we obtain that the order of convergence for the L^∞ norm is N^{-2}. If s is the computational variable for computing the OT mesh, then the L^∞ norm is equidistributed with $r = s^\beta$, so that $dr = \beta s^{\beta-1}ds$. Hence we have $m(r)s^\beta\beta s^{\beta-1}ds = sds \Rightarrow m(r) = 1/\beta(r^{1/\beta})^{2(1-\beta)} = cr^{-2\gamma}$. For the L-shaped domain ($\alpha = 3/2$) we obtain that $\beta = 3$ and $\gamma = 2/3$, whereas for the crack domain ($\alpha = 1/2$) we get $\beta = 4$ and $\gamma = 3/4$. The results derived are in agreement with both Figure 3b and 10b.

A.2 L^2 norm

Following the derivation in [HR11], the optimal mesh density function for piecewise linear interpolation in L^2 norm is

$$\rho = \left(1 + \frac{1}{\kappa}|u''|^2\right)^{1/5}.$$

Ignoring the constant term κ, the equidistribution principle reads as $h\rho = C$ in the limit for $N \to \infty$; so since $|u''| = Kr^{\alpha-2}$

$$h = \frac{dr}{ds} = Kr^{(2-\alpha)\frac{2}{5}}$$

For the L-shaped domain, we have $\alpha = 2/3$ and $h = Kr^{8/15}$, with $\gamma = 8/15 \sim 0.53$. For the crack domain, we have $\alpha = 1/2$ and $h = Kr^{6/10}$, with $\gamma = 3/5$. These results are in agreement with Figure 3a and 10a.

Another critical value for γ can be obtained by dealing with a two-dimensional monitor function. If the solution $u \sim r^{2/3}f(\theta)$, the interpolation error can be expressed as $\delta^2 r\, r^{2/3-2}f(\theta)$ as the skewness is constant close to the origin (Fig. 14b). The L^2_K local estimate of the interpolation error is then proportional to:

$$\mathrm{L}^2_K \sim \delta r\left(\delta^2 r r^{2/3-2}\right) = \delta^3 r r^{-4/3}. \tag{47}$$

The equidistribution of this quantity leads to

$$\left(\frac{dr}{ds}^3\right) r^{-4/3} \sim C \;\Rightarrow\; s \sim r^{5/9} \;\Rightarrow\; m(r) = \frac{s}{r}\frac{ds}{dr} = r^{-8/9}. \tag{48}$$

This gives $\gamma = 4/9$ as the critical exponent for the L-shaped domain and $\gamma = 1/2$ for the crack domain. We remark that this strategy aims at equidistributing the two-dimensional interpolation error. However, this is not ideal for the SIP-dG framework, which seeks to minimise the local truncation error, as evidenced for the critical γ derived via the one-dimensional monitor function (see relative paragraphs in §4.2). Moreover, the estimates η_K (33)-(35) are evaluated along edges, so it is more appropriate to consider the application of an equidistribution strategy in one-dimension.